Vortex-Stretched Flow Around a Cranked Delta Wing

Arthur Rizzi*
FFA The Aeronautical Research Institute of Sweden, Bromma, Sweden
and
Charles J. Purcell†
ETA Systems, Inc., St. Paul, Minnesota

A numerical method that solves the Euler equations for compressible flow is used to study vortex stretching. The particular case simulated is subsonic flow $M_\infty = 0.3$, $\alpha = 10$ deg around a twisted and cambered cranked-and-cropped delta wing. This geometry induces multiple leading-edge vortices in a straining velocity field that brings about flow instabilities, but the result is a state of statistical equilibrium. The discretization contains over 600,000 cells and offers sufficient degrees of freedom in the solution to exhibit the onset of chaotic vortex flow that could well lead to turbulence. The simulated results are compared with wind-tunnel measurements. The agreement at inboard sections is reasonable for the position and strength of the leading-edge vortex; but outboard, it is poor because of the complex transition to disordered vortex flow at the tip. Overall, lift and drag coefficients agree well, however.

Nomenclature

C_D	= drag coefficient
C_L	= lift coefficient
E	= rate-of-strain tensor
e_x, e_y, e_z	= Cartesian unit vectors
FD	= total flux differences
$H(q)$	= $qV + p[0, e_x, e_y, e_z]$ flux
M_∞	= freestream Mach number
n	= unit normal vector
p	= static pressure
p_t	= total pressure
q	= $[\rho, \rho u, \rho v, \rho w]$ variables
u, v, w	= Cartesian components of V
V	= velocity vector
x, y, z	= Cartesian coordinates
α	= angle of attack
ρ	= density
Γ	= artificial viscosity model
ω	= vorticity curl V

Introduction

THE aircraft industry has a practical interest in designing transonic and supersonic vehicles for both military and commercial purposes. A complete analysis of the design of these types of aircraft vehicles is needed in order to establish their feasibility. Today's practical airplane designer relies on wind-tunnel data in order to predict flight characteristics. This paper explores the question of whether a numerical method can simulate the nearly inviscid turbulent flowfield which develops around a wing at the very high Reynolds number of free-flight conditions for use in conjunction with wind-tunnel measurements.

Realistic numerical simulations require three-dimensional discrete models of significant size. The recent construction of a 16-million-word memory for the CYBER 205 has allowed tests of one-million-grid-point models on a practical basis within reasonable elapsed times. Prior to this, it was hoped that this type of computation could be performed with disk I/O, but experience showed that heavy time penalties were encountered due to the demands of the flow-solving algorithm. Therefore, good virtual-memory-management techniques within a sufficient working set of *real* memory seems to be the only effective way to carry out such large-scale simulations. The other crucial requisite is a large bandwidth communication channel between the memory and the arithmetic unit.

As more grid points are added, the accuracy will improve; but, more importantly, from the physical side, the allowable degrees of freedom in the solution will increase so that fundamental flow instabilities, like the interacting of stretched vortices as described by the continuum equations, can be studied. The advent of supercomputers with very large real memory offers the possibility to explore numerically such phenomena.

The type of vortex flowfield to be simulated develops when a delta-shaped wing meets an oncoming stream of air at a high angle of attack. The flow separates from the wing in a shear layer all along the sharp leading edge and, under the influence of the vorticity in the layer, it coils up to form a vortex over the upper surface of the wing. The high velocities in the vortex create a low pressure region under which gives the wing a nonlinear lift. The flow also separates from the trailing edge of the wing in a shear layer which becomes a wake vortex. The primary and wake vortices then interact with each other behind the wing. The appropriate model to describe the fluid mechanics of this vortex flow is the compressible Navier-Stokes equations. But if the Reynolds number of the flow is very large, such as over ten million, the shear stresses and dissipation terms take effect only in very thin layers of the flow on the surface of the wing and across the shear layers that separate from the leading and trailing edges. For this type of flow, it is these free shear layers, and not the boundary layer, that contribute the greatest amount of vorticity. Free-shear layers contain inflexional velocity profiles and are, therefore, subject to inviscid instabilities. Because of the inherent nonlinearity of the equations, it is very difficult to analyze these instabilities, and even more difficult to predict the resulting flow. It is hypothesized that the instabilities are linked to the intensification of vorticity and that this mechanism is an agent in

Received Sept. 19, 1985; presented as Paper 85-4080 at the AIAA 3rd Applied Aerodynamics Conference, Colorado Springs, CO, Oct. 14-16, 1985; revision received Feb. 26, 1986.

*Research Scientist, Aerodynamics Department, Professor, Royal Institute of Technology, Stockholm.
†Principal Consultant.

the transition to chaos and, finally, turbulence. The intent of this paper is to test this hypothesis with a numerical experiment designed to study the dynamics and stability of free-shear layers by means of computer simulation. Because the layers are thin and not influenced by no-slip boundary conditions, the shear stresses and dissipation terms do not have to be accurately represented. They can instead be modeled by simpler nonphysical expressions. In this way, the equations solved are the Euler equations with an artificial-viscosity model. The flow, therefore, is inviscid, except across thin discontinuities like shock waves and vortex sheets that are admitted in the solution where irreversible processes can take place.

Vorticity and Flow Instability

Consider first the simple case of an isolated vortex filament in an inviscid and incompressible fluid. If this single filament is either straight or circular, the dynamics are well known. But give the filament a varying curvature, and immediately it induces a torsion. The coupling of these two phenomena, curvature and torsion, was studied by Betchov.[1] If the vortex filament is plane but of variable curvature, the different segments of the filament will move out of the plane at different velocities. Thus, it acquires torsion.

In general, if a curve moves under the influence of its own segments, two equations can be constructed specifying the evolution of the radius of curvature R and of the torsion T. Betchov studied these equations for the case of a helicoidal filament and found that it moves in space with a translation velocity V_T and rotation producing a tangential velocity V_R. He found two opposing mechanisms in the system of equations: one an intensification of the torsion and the other a dispersion of the torsion. The analysis indicates, however, that the filament may find a statistical equilibrium between the two.

This process describes the way a single filament may reach a distorted but balanced state, and it suggests a mechanism for the transfer of energy from large- to small-scale motion: the so-called energy cascade. In the more general situation, the flow is compressible and contains many vortex filaments which may interact with each other. The dynamics are now much more difficult to analyze and are governed by the vorticity equation for compressible nonisentropic flow

$$\frac{\mathrm{D}}{\mathrm{D}t}\frac{\omega}{\rho}=\frac{\omega}{\rho}\cdot E+\frac{1}{\rho^3}(\text{grad }\rho\times\text{grad }p) \tag{1}$$

where E is the rate-of-strain tensor and $E=\frac{1}{2}(\text{grad } V+\text{grad } V^T)$.

The first term on the right side is the production of vorticity by stretching caused by a straining velocity field, and the second term is produced by nonisentropic processes like shock waves. If both are zero, the ratio ω/ρ is convected unchanged with the fluid element. In the more complicated case, they are nonzero, and under what conditions Eq. (1) may reach some kind of equilibrium is not generally known. Insight into this matter, however, can be achieved by observing the dynamics in numerical simulations. The key questions are whether or not the dynamics of vorticity in Eq. (1) describe a mechanism for the cascade of energy from large to small scales and, in turn, whether these scales are maintained in some statistical equilibrium.

The aim of this paper then is to carry out a numerical experiment to observe the evolution of vorticity according to Eq. (1). When a stream meets a conical delta wing, it separates from the straight leading edge. The vorticity is greatest right at the leading edge; and its direction, given by the leading edge, is primarily along conical rays starting from the apex. To a good approximation, the core of the vortex also lies along one such ray. This fact, together with the conical-flow condition that all radial gradients of velocity vanish, show that the term $\omega\cdot E$ is very nearly zero for such flows. A conical flow therefore is not a good candidate for our experiment. Since the direction of vorticity is so closely governed by the geometry of the leading edge of the wing, a better choice is a wing whose leading edge is curved because this imparts curvature and, hence, torsion to the vortex filaments. In addition to the practical interest in understanding its flowfield, a suitable geometry for the experiment then is a cranked and cropped-delta with camber and twist. Subsonic flow conditions are selected ($M_\infty=0.3$, $\alpha=10$ deg.) for which compressibility effects are strong but do not include shock waves. For this case at least, one of the vorticity production terms on the right side of Eq. (1) should be substantial.

Numerical-Simulation Procedure

Eriksson's method of transfinite interpolation[2] is used to construct a boundary-conforming O-O type mesh with nearly 620,000 cells around the cranked-delta wing (Fig. 1).

The Euler equations can be expressed as an integral balance of the conservation laws

$$\frac{\partial}{\partial t}\int\int\int q\,\mathrm{dvol}+\int\int H(q)\cdot n\,\mathrm{d}s=\int\int\Gamma\,\mathrm{d}s \tag{2}$$

where q is the vector with elements of mass and momentum. The inviscid flux quantity $H(q)\cdot n$ represents the net flux of q transported across, plus the pressure p acting on, the surface S surrounding the volume of fluid. The term Γ is the artificial viscosity model. It has the property of an energy sink, i.e., $(\mathrm{d}/\mathrm{d}t)q^2\le 0$ summed over all cells including those at the boundaries. The finite-volume method then discretizes Eq. (2) by assuming that q is a cell-averaged quantity located in the center of the cell, and the flux term $H(q)\cdot n$ is defined only at the cell faces by averaging the values on each side. With these definitions and calling the cell surfaces in the three coordinate directions of the mesh S_I, S_J, and S_K, the finite-volume form for cell ijk is obtained

$$\frac{\partial}{\partial t}q_{ijk}+[\delta_I(H\cdot S_I)+\delta_J(H\cdot S_J)+\delta_K(H\cdot S_K)]_{ijk}$$
$$=(\delta_I+\delta_J+\delta_K)\Gamma \tag{3}$$

where $\delta_I(H\cdot S_I)=(H\cdot S_I)_{i+\frac{1}{2}}-(H\cdot S_I)_{i-\frac{1}{2}}$ is the centered difference operator. A more detailed description of the method is given in Ref. 3. With the appropriate boundary conditions, this last equation is integrated with the two-level three-stage scheme

$$q_0=q$$
$$q=q_0+\Delta t FD(q_0)$$
$$q=q_0+\Delta t[\tfrac{1}{2}FD(q_0)+\tfrac{1}{2}FD(q)]$$
$$q=q_0+\Delta t[\tfrac{1}{2}FD(q_0)+\tfrac{1}{2}FD(q)]$$

that steps the solution forward in time.

Data Structure and Methodology for Vector Processing

The nature of the vector instructions in current supercomputers emphasizes rapid operations upon contiguous cells in memory. A three-dimensional structure suitable for vector processing is correctly visualized as consisting of a collection of adjacent pencils with memory cells and suitable boundary conditions. In conjunction with the data-structure design, key features of the vector-processing procedure are the following: 1) separate storage arrays are assigned for the

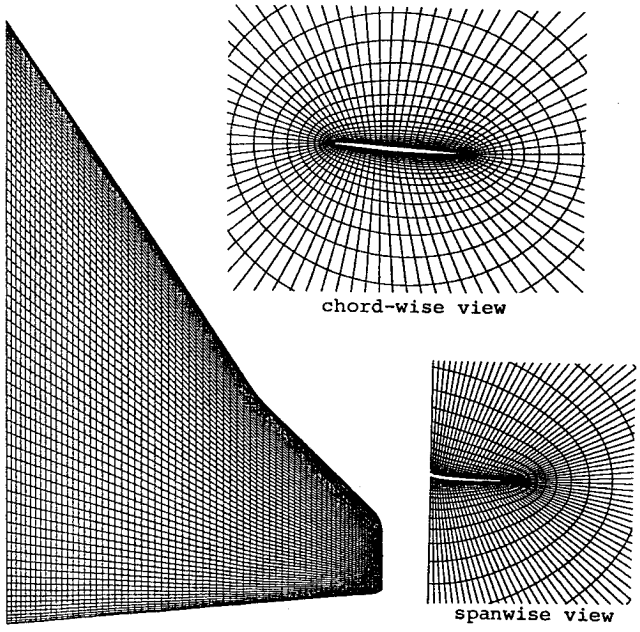

Fig. 1 O-O type mesh with $160\times48\times80$ cells around a cranked delta wing.

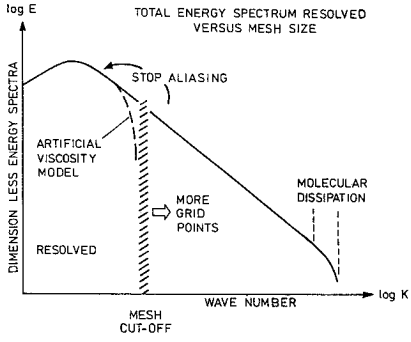

Fig. 2 Energy cascade of a high-Reynolds-number turbulent flow. If the mesh dimensions are large enough, it may be possible to approximate the overall effects of small-scale instabilities.

dependent variables q, flux component F, and flux differences FD; 2) one extra unit is dimensioned for each computational direction to hold the boundary conditions; and 3) flux differences are taken throughout the entire field by offsetting the starting location of the flux vector F. In this way, all of the work in updating interior points is exclusively vector operations without any data motion. The vector lengths obtained are long, containing about 50,000 elements, and span three-dimensional subsets of the data. This high degree of vectorization allows processing very large data sets most effectively.

Simulated Vortex Flowfield

The flow model that we have described dissipates phenomena whose wavelength is on the order of the mesh spacing, so it mimics the action of the real Newtonian viscosity which acts on the molecular scale for high-Reynolds-number flows. Therefore, the smaller the mesh spacing, the finer the scale-length of the phenomena that can be resolved without it being obliterated by the numerical dissipation. If there is an energy cascade at work in the flow, it will only be seen in very dense meshes (Fig. 2). The standard mesh dimensions, about 60,000 cells, can support only

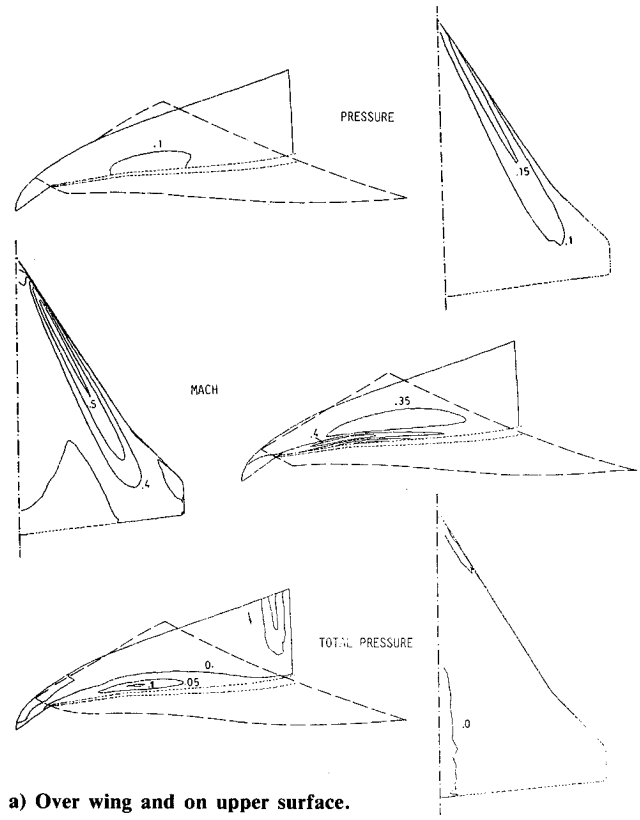

a) Over wing and on upper surface.

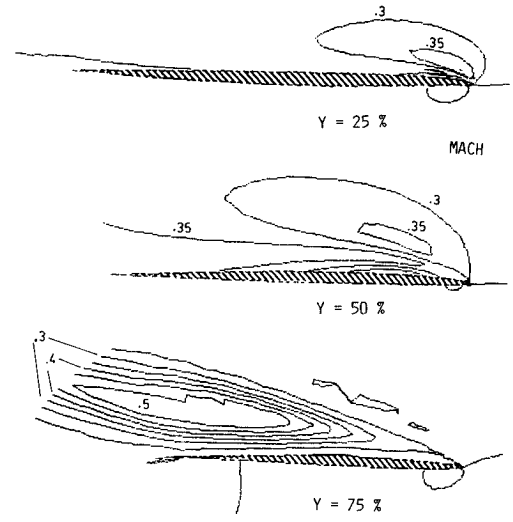

b) Mach number in three chordwise sections.

Fig. 3 Flowfield computed with the standard mesh of $80\times24\times40$ cells, $M_\infty=0.3$, $\alpha=10$ deg. Contours of normalized pressure $1\text{-}p/p_{t_\infty}$, Mach number, and total pressure $1\text{-}p_t/p_\infty$.

the steady large-scale features; many such simulations have been carried out before. Given a sufficient number of grid points to support the small scales, the Euler equations may model vortical flow instabilities which under suitable conditions can be statistically steady and consistent, at least in an average sense, with the coarser-grid solution. The mechanism for the excitation, as well as the probable instability of the small-scale flow features sustained by the transfer of energy from the large scales, is the stretching of vorticity caused by the external straining of the free shear layers in this flow. The following computed results for flow around the wing at $M_\infty=0.3$, $\alpha=10$ deg support this argument.

Figure 3a presents contours of the simulated flow on the upper surface of the wing and in one spanwise plane over it. These are results obtained with a standard mesh size of 80 cells around the chord, 40 across the span, and 24 outward. Figures 3a and 3b indicate a laminar vortex flow much like the ones simulated previously. The isobars and isoMach contours show that a vortex does form from the free-shear layer shed from the leading edge, but the footprint of the vortex weakens just beyond the crank, where it might have been expected that another vortex would form, or, at least, the core would curve. Losses in total pressure are mostly found in the vortex core, for reasons now understood,[4] and shock waves do not contribute to the vorticity in this case. The lift and drag coefficients are $C_L = 0.5503$ and $C_D = 0.930$. This standard-mesh solution is presented in order to portray the large-scale motion and to provide a basis for comparison with the fine-mesh results.

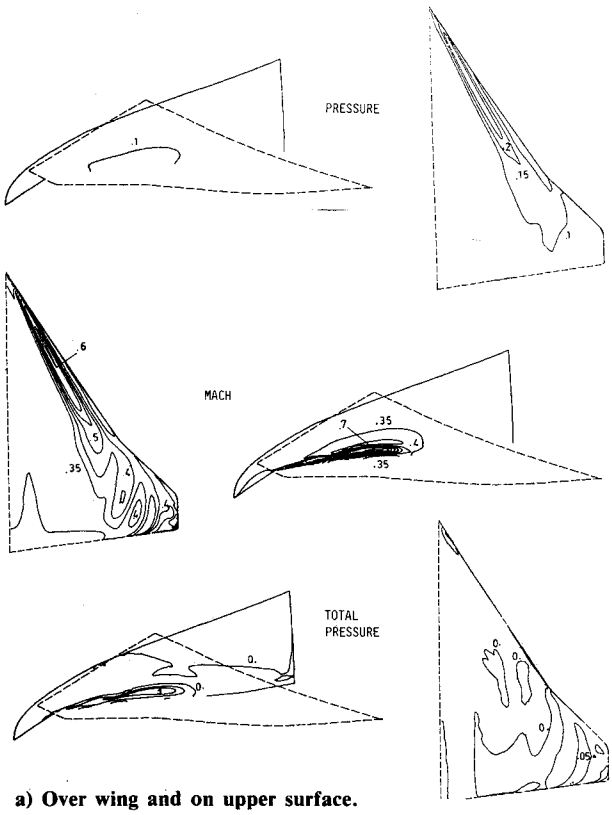

a) Over wing and on upper surface.

The solution obtained on a mesh having double the number of cells in each of the coordinate dimensions ($160 \times 48 \times 80$) as the standard mesh is given in Figs. 4a and 4b. The most striking differences between Fig. 3a and Fig. 4a show up in the isobars and isoMach contours of the vortex footprint in the vicinity of the crank. Instead of diminishing, the contours in Fig. 4a suggest a wave character not seen in the standard mesh. Also, over the wing, more small-scale features appear in the vortex core, as evidenced by the contours of Mach number and total pressure loss. It is believed that this small-scale structure comes from the torsional forces brought about by the curving of the vortex filaments. One effect of this (Fig. 4b) is a helicoidal plume in the isoMach contours in the chord section near the crank. It is only possible to support scales like these on a fine mesh. A further refined mesh may well reveal even smaller ones. The destabilizing forces that bring about this motion, however, do seem to be in equilibrium with the overall flow. The integrated forces $C_L = 0.5499$ and $C_D = 0.0894$ are only slightly different from the standard-mesh values and compare favorably with the values $C_L = 0.53$ and $C_D = 0.086$ measured in a wind-tunnel experiment.

Figure 5 contains the chordwise comparison at four span locations of the surface pressure computed in the standard and fine meshes with those measured in the wind tunnel.[5] (Because it is so thin, the tip section of the model contains only upper-surface taps.) The physical model includes a fuselage, but the numerical one does not. On the lower surface the agreement of all three results is quite good. On the upper surface and inboard sections at $y/b = 0.25$ and 0.50 show

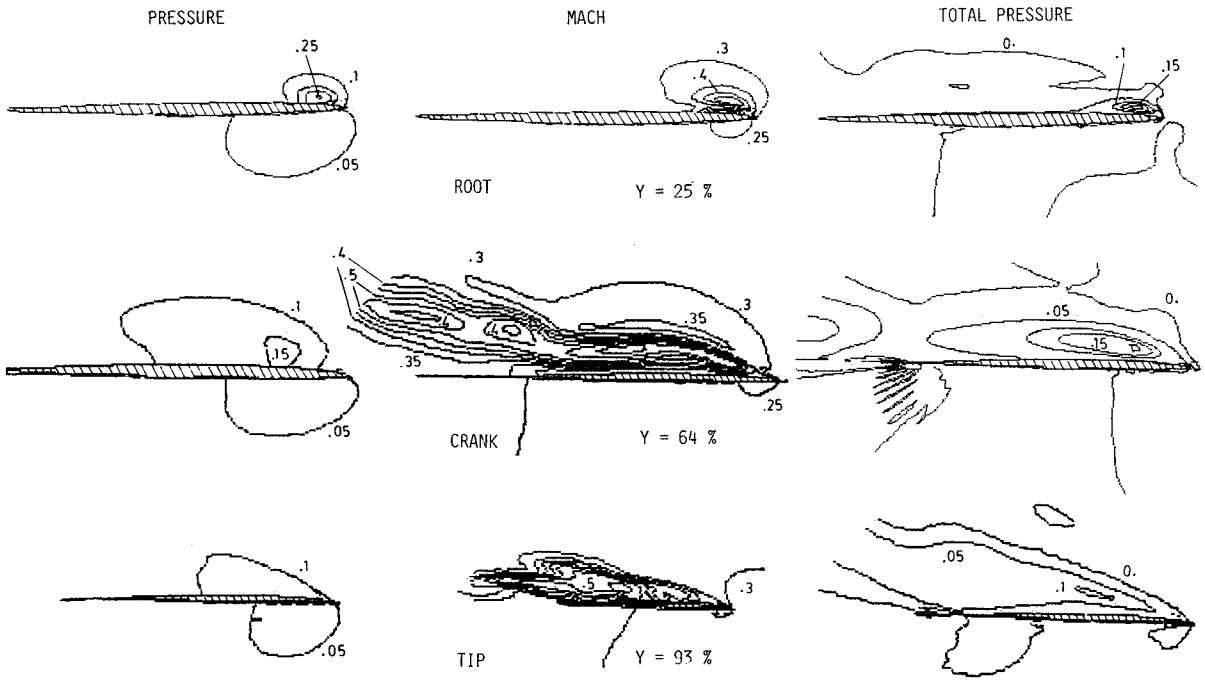

b) Three chordwise sections.

Fig. 4 Flowfield computed with fine mesh of $160 \times 48 \times 80$ cells. $M_\infty = 0.3$, $\alpha = 10$ deg. Contours of normalized pressure $1\text{-}p/p_{t_\infty}$, Mach number, and total pressure $1\text{-}p_t/p_\infty$.

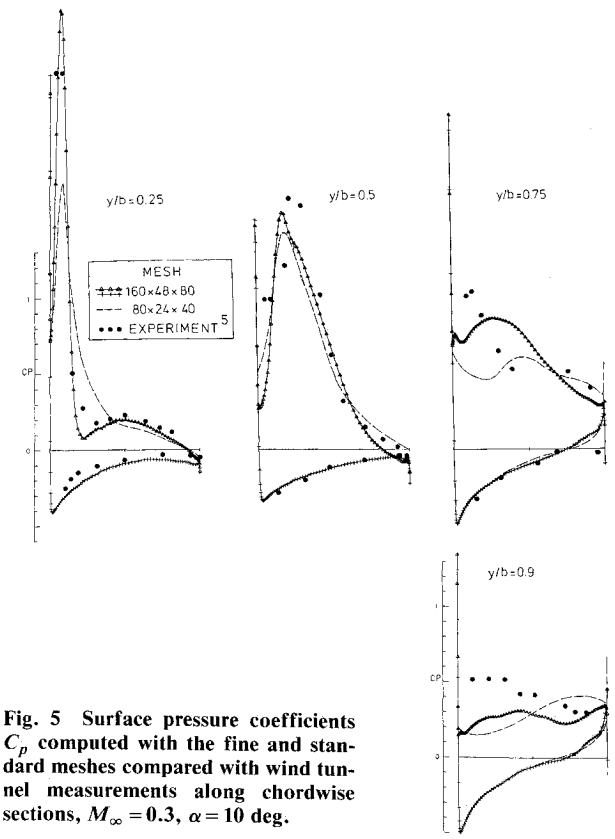

Fig. 5 Surface pressure coefficients C_p computed with the fine and standard meshes compared with wind tunnel measurements along chordwise sections, $M_\infty = 0.3$, $\alpha = 10$ deg.

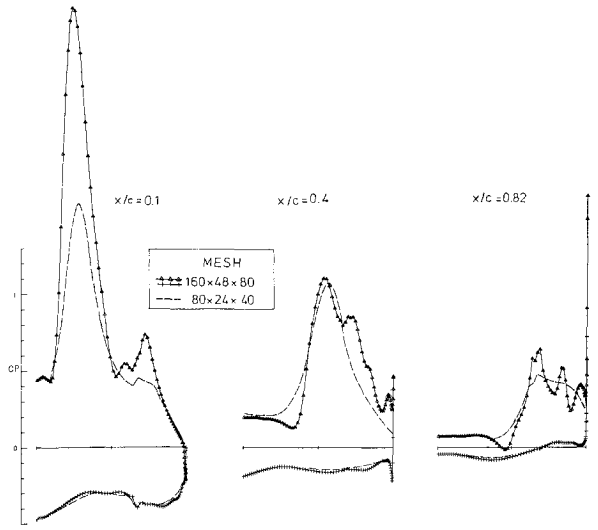

Fig. 6 Spanwise comparisons of the standard-mesh and fine-mesh results for surface pressure.

good agreement for the position and strength of the vortex as evidenced by the suction peaks it produces. The agreement in the next two sections is considerably worse, however. Near the crank at $y/b = 0.75$ no discernible vortex suction peak is found in the standard-mesh results. The fine-mesh results do show such a peak but it is weaker and broader and somewhat downstream of the measured one. In the tip section $y/b = 0.9$, there are no peaks in either the computed or the measured values, and this suggests the absence of a coherent vortex. Quantitatively, however, both sets of computed pressures differ from the measured values by as much as a factor of two at the leading edge. Possible explanations for this discrepancy may be the influence of the fuselage of the model, including the shedding of nose vortices and aeroelastic effects at the tip of the model. It seems more likely, however, that the flow in these two sections are undergoing a complex transition from a coherent leading-edge vortex inboard to a disordered vortex flow at the tip, and it is difficult to model this situation. But given all the assumptions made, it is encouraging to see that the model is realistic enough to show improved detail in the comparison of the pressure distributions as the mesh is refined. For flows at low angle of attack the numerical model also has produced results in good agreement with a panel method.[6] The spanwise comparison (Fig. 6) brings out the differences in the standard and fine mesh solutions. Inboard of the crank, the fine-mesh solution shows a better representation of the vortex; outboard of the crank, it reveals that the instabilities cause the fine-mesh pressure to oscillate around the standard-mesh values.

Final Remarks

Vortical flows are among the most baffling for the fluid dynamicist to understand. They are susceptible to instabilities, can develop local regions of extreme velocity and vorticity, and are inherently nonlinear. They are therefore prime subjects for numerical study. Here one aspect of vortical flow, the bending or curving of vortex filaments brought on by the geometry of the boundary that determines the flow, has been studied. With sufficient degrees of freedom given to the solution by the mesh size, small-scale torsional-wave effects due to a cranked leading edge have been observed in a flowfield which is in overall equilibrium. Wind tunnel measurements verify that the results of the numerical simulation bears a certain amount of realism. Further study is obviously required for this type of flowfield.

Acknowledgments

The authors thank P. Sacher of MBB-Ottobrunn for suggesting that we study this flow around the TKF wing, and G. Cucinelli of MBB-Ottobrunn for his assistance in evaluating the results and comparing them with the experiments. The computer time provided by the Control Data Corporation to carry out these computations on its large-memory CYBER 205 is gratefully acknowledged.

References

[1]Betchov, R., "On the Curvature and Torsion of an Isolated Vortex Filament," *Journal of Fluid Mechanics,* Vol. 22, July 1965, pp. 471-479.

[2]Eriksson, L. E., "Generation of Boundary-Conforming Grids Around Wing-Body Configurations using Transfinite Interpolation," *AIAA Journal,* Vol. 20, Oct. 1982, pp. 1313-1320.

[3]Rizzi, A. W. and Eriksson, L. E., "Computation of Flow Around Wings Based on the Euler Equations," *Fluid Mechanics,* Vol. 148, Nov. 1984, pp. 45-71.

[4]Powell, K., Murman, E., Perez, E., and Baron, J., "Total Pressure Loss in Vortical Solutions of the Conical Euler Equations," AIAA Paper 85-1701, 1985.

[5]Le Fauga, A., "Untersuchungen des elastischen Verhaltens eines sogenannten starren Windkanalmodells," *MBB Report,* LKE 294-ACA-R24, Munich, FRG, 1982.

[6]Fornasier, L., and Rizzi, A., "Comparisons of Results from a Panel Method and an Euler Code for a Cranked Delta Wing," AIAA Paper 85-4091, 1985.